JOURNAL OF GEOPHYSICAL RESEARCH, VOL. 114, B05309, doi:10.1029/2008JB006011, 2009

Aftershock modeling based on uncertain stress calculations

S. Hainzl,[1] B. Enescu,[1,2] M. Cocco,[3] J. Woessner,[4] F. Catalli,[3] R. Wang,[1] and F. Roth[1]

Received 12 August 2008; revised 2 March 2009; accepted 19 March 2009; published 28 May 2009.

[1] We discuss the impact of uncertainties in computed coseismic stress perturbations on the seismicity rate changes forecasted through a rate- and state-dependent frictional model. We aim to understand how the variability of Coulomb stress changes affects the correlation between predicted and observed changes in the rate of earthquake production. We use the aftershock activity following the 1992 M7.3 Landers (California) earthquake as a case study. To accomplish these tasks, we first analyze the variability of stress changes resulting from the use of different published slip distributions. We find that the standard deviation of the uncertainty is of the same size as the absolute stress change and that their ratio, the coefficient of variation (CV), is approximately constant in space. This uncertainty has a strong impact on the forecasted aftershock activity if a rate-and-state frictional model is considered. We use the early aftershocks to invert for friction parameters and the coefficient of variation by means of the maximum likelihood method. We show that, when the uncertainties are properly taken into account, the inversion yields stable results, which fit the spatiotemporal aftershock sequence. The analysis of the 1992 Landers sequence demonstrates that accounting for realistic uncertainties in stress changes strongly improves the correlation between modeled and observed seismicity rate changes. For this sequence, we measure a friction parameter $A\sigma_n \approx 0.017$ MPa and a coefficient of stress variation $CV = 0.95$.

Citation: Hainzl, S., B. Enescu, M. Cocco, J. Woessner, F. Catalli, R. Wang, and F. Roth (2009), Aftershock modeling based on uncertain stress calculations, *J. Geophys. Res.*, *114*, B05309, doi:10.1029/2008JB006011.

1. Introduction

[2] Aftershocks are commonly seen as the delayed response of a fault population to static Coulomb stress changes (ΔCFS) induced by a main shock [see, e.g., *Harris*, 1998; *Stein*, 1999; *Steacy et al.*, 2005a; M. Cocco et al., Sensitivity study of forecasts based on Coulomb stress calculation and rate- and state-dependent frictional response, submitted to *Journal of Geophysical Research*, 2009, hereinafter referred to as Cocco et al., submitted manuscript, 2009]. By joining the coseismic stress changes with the rate- and state-dependent frictional response of a population of nucleating patches [*Dieterich*, 1994], both the spatial distribution of aftershocks and their temporal decay can be modeled. In particular, it explains the empirical Omori-Utsu law

$$\lambda(t) = \frac{K}{(t+c)^p} \tag{1}$$

where t indicates the elapsed time since the main shock; K, c and p are constants where c is typically found to be much less than 1 day and the p value is between 0.8 and 1.2 for most cases [*Utsu et al.*, 1995]. For a population of faults in the nucleation regime, a sudden stress jump leads to a nonlinear response of earthquake nucleation times which matches the Omori-Utsu law with $p = 1$ until the seismic activity returns to the background level [*Dieterich*, 1994; Cocco et al., submitted manuscript, 2009]. Applications of this model to empirical data provided a good explanation of the observations [*Dieterich et al.*, 2000; *Toda et al.*, 2002, 2005; *Hainzl et al.*, 2006], and reasonable estimations for the regional stressing rate [*Gross and Kisslinger*, 1997; *Gross*, 2001].

[3] However, the observation of aftershocks occurring in stress shadows, i.e., in regions where the calculated stress change becomes negative, $\Delta CFS < 0$, seems to contradict the stress triggering mechanism [*Hardebeck et al.*, 1998; *Catalli et al.*, 2008]. Regions of reduced activity, as predicted by the static stress triggering model for stress shadows, are hardly found in real data and might even not exist [*Marsan*, 2003]. Indeed, it has been recently demonstrated that accounting for the small-scale slip variability that might not be accessible to direct measurement, can explain the absence of regions of quiescence in the first period of the aftershock activity [*Helmstetter and Shaw*, 2006; *Marsan*, 2006].

[4] All applications of the stress-triggering model rely on the determination of the induced stress changes. However,

[1]GFZ German Research Centre for Geosciences, Potsdam, Germany.
[2]Now at Earthquake Research Department, National Research Institute for Earth Science and Disaster Prevention, Tsukuba, Japan.
[3]Instituto Nationale di Geofisica e Vulcanologia, Rome, Italy.
[4]Institute of Geophysics, ETH Zurich, Zurich, Switzerland.

0148-0227/09/2008JB006011$09.00

the stress calculation consists of unsolved problems which lead to large uncertainties such as (1) the unknown distribution of receiver faults [*McCloskey et al.*, 2003; *Steacy et al.*, 2005b]; (2) the nonunique inversion results for the slip models [*Steacy et al.*, 2004]; (3) uncalculable small-scale slip variability which can lead to strong stress heterogeneities close to the source fault [*Marsan*, 2006; *Hainzl and Marsan*, 2008], and (4) spatial inhomogeneity of material and prestress conditions. *Marsan and Daniel* [2007] tried to estimate the stress variability directly from seismicity data without calculating the main shock induced stress changes. For certain areas surrounding the 1999 Chi-Chi earthquake, they found that the estimated variability is on the order of the estimated mean stress change and partially even larger.

[5] In this paper, we now take the aleatoric and epistemic uncertainties of deterministically calculated stresses directly into account. We show that considering the stress uncertainties in aftershock modeling is crucial for obtaining stable parameter estimations and good fits of the aftershock activity. To this goal, we examine the well-studied case of the 1992 M7.3 Landers, California, earthquake which offers the possibility to systematically compare stress variability resulting from a number of different published slip distributions. In a simplified way, we account for this variability in the maximum likelihood estimation of the model parameters. Finally, we show that the resulting model based on rate-and-state frictional behavior can well explain the main features of the temporal decay of Landers aftershocks and their spatial distribution.

2. Uncertainty of Stress Calculations

[6] The Landers earthquake ($M_w = 7.3$) occurred on June 28, 1992 with an epicenter located at $-116.44°$ longitude and $34.20°$ latitude. It triggered an intense aftershock activity of more than 700 $M \geq 3$ events within the first 10 days (see the earthquake catalogue by *Hauksson et al.* [2003]). Its largest aftershock, the M_w6.4 Big Bear event, occurred approximately 4 hours after the main shock. In the following, we will analyze the stress changes related to the Landers and Big Bear earthquakes. In particular, we will quantify the variability of the stress values determined by alternative slip models and reasonable assumptions about the involved parameter uncertainties.

2.1. Static Coulomb-Stress Changes

[7] Coulomb stress changes are defined according to the relation

$$\Delta CFS = \Delta\tau + \mu(\Delta\sigma_n + \Delta P) \quad (2)$$

where $\Delta\tau$ are the shear stress changes calculated along the slip direction on the assumed fault plane, $\Delta\sigma_n$ are the normal stress changes (positive for extension), μ is the friction coefficient and ΔP indicates the pore pressure changes [e.g., *Harris*, 1998]. In this study, we use the constant apparent friction model [*Cocco and Rice*, 2002; Cocco et al., submitted manuscript, 2009], according to which the Coulomb-stress changes can be written as $\Delta CFS = \Delta\tau + \mu'\Delta\sigma_n$, where $\mu' = (1 - B)\,\mu$ and B is the Skempton coefficient which varies between 0 and 1 [*King et al.*, 1994; *Beeler et al.*, 2000; *Cocco and Rice*, 2002]. In the following, the effective friction coefficient is set to 0.3 which is consistent with the assumption that the Landers main shock rupture is approximately optimally oriented to the external stress field assumed to be a uniaxial compressional stress of 10 MPa oriented N7 E [*King et al.*, 1994; *Hardebeck and Hauksson*, 2001].

[8] Several different slip models for the Landers earthquake have been published so far. In the following, we use all five models available in the finite-source rupture model database maintained by Martin Mai (see http://www.seismo.ethz.ch/srcmod/) to calculate the stress changes induced by the main shock; i.e., the slip models of (1) *Wald and Heaton* [1994]; (2) *Hernandez et al.* [1999]; (3) *Cotton and Campillo* [1995]; (4) *Cohee and Beroza* [1994]; and (5) *Zeng and Anderson* [2000]. Whereas the latter three inversions are solely based on strong motion data, the former two also inverted GPS displacements.

[9] In each case, we calculated the coseismic stresses using the code of *Wang et al.* [2006]. For each slip model, we used the layered velocity and density structure that has been previously used to invert the slip model (see the finite-source rupture model database). In addition to the Landers main shock, we also considered the stress changes induced by its largest aftershock, namely the M6.4 Big Bear event, for which we used the two-segment slip model inverted by *Jones and Hough* [1995].

[10] The Coulomb stress changes can be computed on prescribed receivers or on Optimally Oriented Planes for Coulomb failure (OOPs). The OOPs are characterized by the strike, dip and rake values that maximize *CFS* with regard to the total stress tensor defined as $\sigma^{tot} = \sigma^r + \Delta\sigma$. Here σ^r is the regional stress field and $\Delta\sigma$ is the coseismic stress perturbation. As pointed out by Cocco et al. (submitted manuscript, 2009), stresses increase close to the causative fault if they are resolved onto optimally oriented fault planes whereas they are predicted to decrease (stress shadow) when resolved on prescribed receivers which are oriented in the same way as the main shock. Figure 1a shows an example of a stress distribution at 7 km depth computed for OOPs. While none of both possible scenarios (the existence of only one receiver mechanism or the preexistence of all possible fault orientations) is entirely realistic, stress changes calculated for optimal oriented fault planes are more appropriate to explain the observation that seismicity is almost everywhere activated [*Marsan*, 2003]. This qualitative result is confirmed by the fact that the maximum likelihood method (described in section 3.3) yields significantly higher likelihood values for OOPs. Therefore we discuss here only the results for stress changes calculated on OOPs.

2.2. Variability of Stress Values

[11] The five different slip models lead to quite different estimations of stress values at different locations. To illustrate this, we calculated the standard deviation of the five stress values at each grid point. In a map view, Figure 1 shows the mean stress change and the standard deviation at 7 km depth. The patterns and absolute values of the stress change, as well as the standard deviation are quite similar. This implies that the standard deviation of the five stress

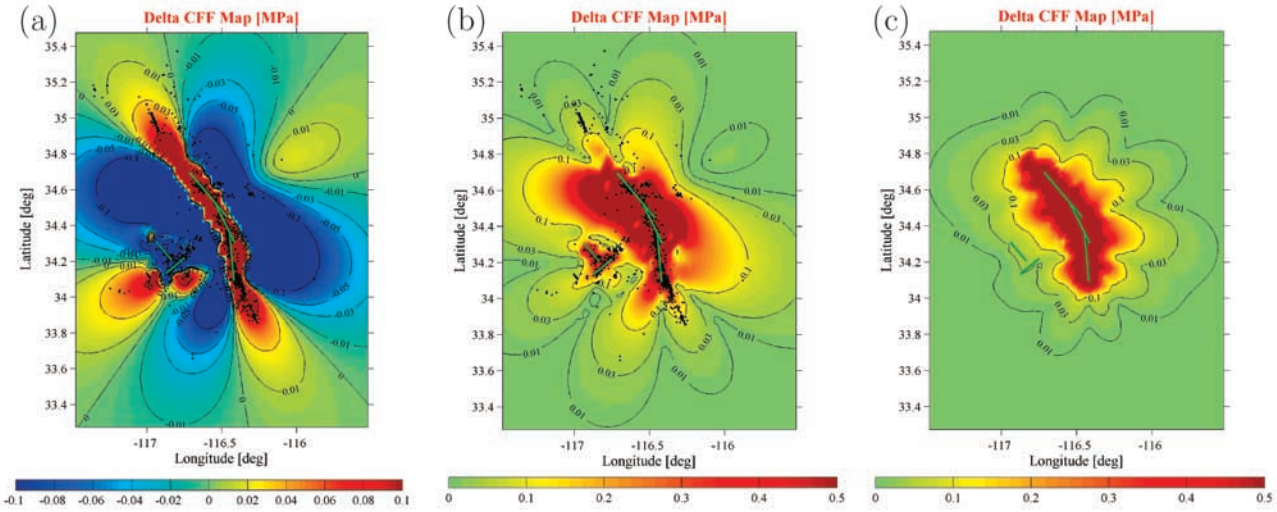

Figure 1. Map of the earthquake distribution (dots) after the Landers main shock (bold lines indicate the *Wald and Heaton* [1994] fault trace) in comparison with Coulomb-stress changes ΔCFS at 7 km depth: (a) mean value of the stress changes $\langle \Delta CFS \rangle$; (b) absolute value of the stress changes $|\langle \Delta CFS \rangle|$; and (c) standard deviation of the stress values calculated from the five different slip models.

change estimations is on the same order as the mean stress change at each location.

[12] The scattering of the stress values calculated from the different published slip inversions represents roughly the epistemic uncertainty of our stress calculation, or in other words, the uncertainty related to our limited knowledge of the true coseismic slip distribution. However, the probability distribution of stresses in each subvolume is expected to scatter also due to several other reasons. For example, the direction and amplitude of the regional stress field [*Hardebeck and Hauksson*, 2001], as well as the orientation of preexisting receiver faults at depth are only poorly constrained, and there might be significant local variations of the prestress due to material heterogeneities and precursory earthquakes.

[13] Now we would like to explore the expected stress variability which results from reasonable assumptions about the involved model uncertainty and variability. We randomly selected 20 locations with a significant negative average stress change and 20 locations with a significant positive stress change. At these locations, we performed 1000 different randomized stress calculations for each of the five slip inversions. The parameters for these stress calculations were selected randomly from Gaussian distributions around their original values. All selected parameters together with their standard deviations are listed in Table 1. The chosen values are not directly based on estimations from the slip inversions because such information is commonly not provided. However, they are in reasonable agreement with estimations for the regional stress field [*Hardebeck and Hauksson*, 2001] and general slip uncertainties [*Hartzell et al.*, 2007].

[14] The resulting distributions for four representative examples are shown in Figure 2. It can be seen that the average distribution can be quite well fitted at each location with a Gaussian distribution. However, note that a more appropriate analysis of the true shape of the error function would require the incorporation of probability distributions directly derived from the individual slip inversions.

[15] For all 40 locations, the calculated standard deviation δ of the resulting distribution is shown in Figure 3 as a function of the mean stress change. It is found that the variability of the stress estimation is, in a first approximation, linearly correlated to the value of the absolute mean stress change $|\langle \Delta CFS \rangle|$, indicating that the coefficient of variation $CV = \delta / |\langle \Delta CFS \rangle|$ is approximately constant in space. Such a constant relative error is generally expected in the case of linear systems. Furthermore, the CV value is found to be on the order of 1 for these stochastic calculations. Note that this is only a rough estimation because of our rather arbitrary choices of the involved uncertainties. However, we will see in the next section that the inversion of the aftershock data yields a similar estimation of CV.

3. Aftershock Probabilities Based on Coseismic Stress Changes

3.1. Application of the Rate-and-State Frictional Fault Population Model

[16] We relate stress changes to earthquake rates using the framework of rate-and-state friction [*Dieterich*, 1994; *Dieterich et al.*, 2000] which properly takes into consideration the rate and slip dependence of frictional strength and

Table 1. Summary of the Input Parameters for the Randomized Stress Calculations

	Mean	Standard Deviation
Compressional stress	10 MPa	4 MPa
Uniaxial stress direction	N7°E	10°
Friction coefficient	0.3	0.1
Strike of fault segments	defined for each model	3° (rotation around central point)
Dip of fault segments	defined for each model	3°
Slip direction (rake)	defined for each patch	5°
Slip	defined for each patch	30% relative error

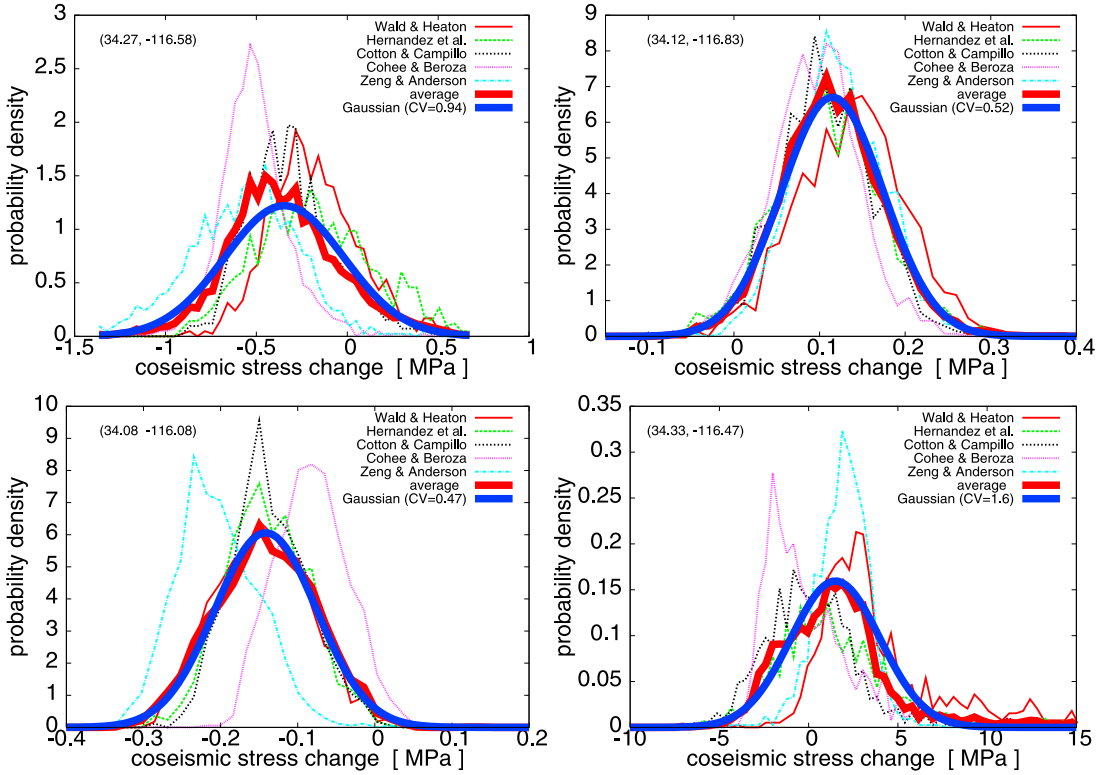

Figure 2. The plots show the probability distributions of the stress changes at four selected locations (34.27°, −116.58°; 34.12°, −116.83°; 34.08°, −116.08°; and 34.33°, −116.47°; respectively) for the five different published slip models with randomly added perturbations (see Table 1). Additionally, the averaged and the approximated Gaussian distributions are shown (bold lines).

time-dependent restrengthening observed in laboratory experiments. According to this theory, the seismicity rate R is inversely proportional to the state variable γ describing the creep velocities on the faults, namely

$$R(t) = \frac{r}{\dot{\tau}\gamma} \tag{3}$$

where r is the stationary background rate and $\dot{\tau}$ the tectonic loading rate. The evolution of the state variable as a function of infinitesimal changes of time dt and stress $d\tau$ is given by

$$d\gamma = \frac{dt - \gamma d\tau}{A\sigma_n} \tag{4}$$

with A being a dimensionless fault constitutive parameter usually ∼0.01 [*Dieterich*, 1994; *Dieterich et al.*, 2000]. If normal stress changes are small compared to the absolute value σ_n, the same evolution law, i.e., $d\gamma = (dt - \gamma dS)/A\sigma_n$, holds also for the stress value: $S = \tau + (\mu - \alpha)(\sigma_n + p)$. Here α is a positive nondimensional parameter controlling the normal stress changes [*Linker and Dieterich*, 1992]. This parameter is commonly set to 0.25. Because the constant apparent friction model (see above) leads to $S = \tau + \mu_{eff}\sigma_n$, the function S is equal to the Coulomb-stress with an effective friction coefficient of $\mu_{eff} = (\mu - \alpha)(1 - B)$ (see discussion in *Catalli et al.* [2008]). For our calculations, we set $\mu_{eff} = 0.3$. For a sequence of stress jumps, the evolution law (equation (4)) can be solved by iteration (see section A1).

[17] Thus the rate-and-state model consists of 3 parameters which can be defined as (1) background rate r, (2) aftershock relaxation time $t_a \equiv A\sigma_n/\dot{\tau}$, and (3) frictional resistance $A\sigma_n$.

[18] In general, these values are not known and have to be estimated from the observed seismicity data or using some

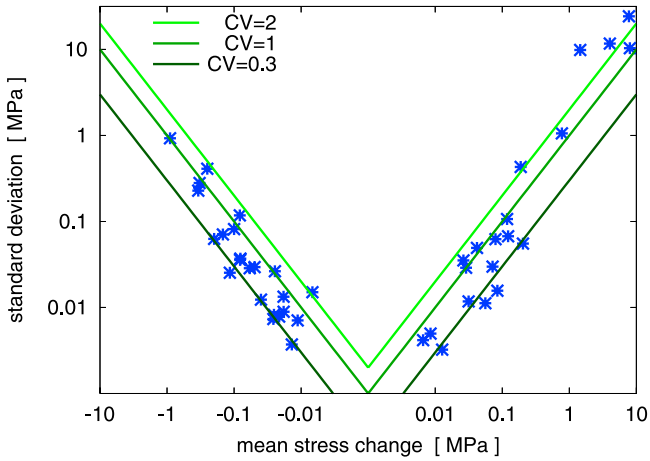

Figure 3. Standard variation of calculated stress changes as a function of the mean stress change. The result is plotted for the 40 randomly selected locations where we have calculated the stresses based on the uncertainties given in Table 1. The lines correspond to different values of the coefficient of variation CV.

approximate physical relations [see detailed discussion in Cocco et al. (submitted manuscript, 2009)].

[19] The variability, respectively uncertainty, of each stress jump can be taken into account by averaging over a large number of Monte Carlo simulations of random possible stressing histories. As described in more detail in the appendix, each of these synthetic stressing histories consists of stress jumps randomly selected from Gaussian distributions, $f(\Delta S) = \exp(-(\Delta S - \langle \Delta S \rangle)^2/2\delta^2)/\sqrt{2\pi}\delta$, where the mean value is indicated by $\langle\rangle$ and the standard deviation δ is proportional to the absolute value of the mean stress change at that location, i.e., $\delta = CV \cdot \sqrt{\langle \Delta S \rangle^2}$. Thus we have only one additional model parameter CV accounting for the stress variability in all places. The assumed linear correlation between the standard deviation and the stress level seems to be justified by our results described in section 2.1 (see Figure 3).

[20] To guarantee a good sampling of the probability distribution, the number of Monte Carlo simulations should increase with the number of stress steps. For the following investigations, we used the two stress steps related to the M7.3 Landers main shock and its largest aftershock, the M6.4 Big Bear earthquake, and performed in general 100 simulations for each location. However, we checked the robustness of our results using also a larger number of 1000 Monte Carlo simulations.

3.2. Aftershock Data

[21] We analyzed the relocated earthquake catalogue of *Hauksson et al.* [2003] for the region −117.5°W to −115.5°W and 33.25°N to 35.5°N (SCEDC webpage at http://www.data.scec.org/research/altcatalogs.html). To ensure a complete earthquake recording, we only used aftershocks with magnitudes $M \geq 3$ [*Woessner and Wiemer*, 2005]. Furthermore, we neglected aftershocks that occurred within the first 12 hours after the Landers earthquake to account for likely incomplete catalogue recordings in the first time interval [*Kagan*, 2004]. The aftershocks included in earthquake catalogues can be typically fitted with a c value of the Omori-Utsu law which is in the order of minutes to hours. Recent attempts to find a c value which is of physical rather than instrumental origin have proposed that it could be only in the order of one to several minutes [*Kagan and Houston*, 2005; *Peng et al.*, 2006, 2007; *Enescu et al.*, 2007, 2009], although there is no clear consensus of how the Omori-Utsu law actually breaks down below this cutoff. However, because we are dealing with a standard earthquake catalogue and our model does not account for incomplete recordings, we cut the first part of the sequence. We chose 12 hours in agreement with the estimation of *Helmstetter et al.* [2005] for the time of incompleteness for $M \geq 3$ earthquakes in southern California.

3.3. Parameter Estimation

[22] Assuming that the model parameters are constant in space, our model consists of 4 free parameters which have to be estimated from the data: t_a, $A\sigma_n$, r, and CV. We carried out the data fitting using the maximum likelihood method [*Ogata*, 1998; *Daley and Vere-Jones*, 2003]. In the section A2, it is discussed in detail how this method has been implemented for our case. Note that we used for this estimation the stress changes calculated for 15 different layers within 1 and 15 km depth and on a horizontal grid with spacing of 0.05°.

[23] The parameter t_a is essentially defining the time relative to the main shock when the Omori decay bends into the constant background rate r. Thus this parameter is poorly constrained by the first year aftershocks. Varying t_a leads mainly to a rescaling of the other parameters as shown by Cocco et al. (submitted manuscript, 2009). We estimated the best t_a value using the first 100 days aftershocks and found a broad likelihood maximum between 15 and 40 years. However, the decrease of the log likelihood values for t_a values larger than 40 years is quite weak and the difference between the maximum and the value for, e.g., t_a = 100 years is small. To reduce the parameter space, we therefore fixed the aftershock duration time to the value of t_a = 10000 days ≈ 27.4 years. For a comparison of a less likely but still possible larger value, we repeated all estimations for the value t_a = 100 years. The remaining parameters which are fitted by the maximum likelihood method are $A\sigma_n$, r, and CV.

[24] We estimated the model parameters after each 24 hours subsequent to the Landers main shock time t_M, i.e., at times $T_i = t_M + i$ days, on basis of the preceding aftershock activity. However, the maximization of the log likelihood function (equation (A3)) was done only for aftershocks occurred after the first 12 hours (i.e., within $[t_M + 0.5, T_i]$) to account for possible incompleteness of the recordings in the first time interval (see above). The results are shown in Figure 4. In the case that the uncertainty/variability of the estimated stress changes is ignored, i.e., if CV is set to 0, we find that the estimations are not stable. In particular, both $A\sigma_n$ and r are estimated to be extremely high directly after the main shock indicating that the best solution is an almost constant aftershock probability in space. Because of the Omori-type aftershock decay, the estimated background rate and thus the total rate becomes rapidly smaller if longer aftershock time periods are taken into account. In contrast, if the stress heterogeneities are considered by means of the parameter CV, all parameters are already well constrained by the first day aftershocks and remain stable for estimations based on much longer time intervals. This indicates that, in this case, no systematic bias exists in the model estimation.

[25] The estimated value of $A\sigma_n \approx 0.017$ MPa is in the same order as previous estimations: e.g., $A\sigma_n = 0.035 \pm 0.015$ MPa for the 1995 M_w6.9 Kobe earthquake [*Toda et al.*, 1998]; $A\sigma_n = 0.01$ MPa for the 2000 Izu earthquake swarm [*Toda et al.*, 2002]; $A\sigma_n = 0.04$ MPa for the 1997 Umbria-Marche sequence in central Italy [*Catalli et al.*, 2008]; and $A\sigma_n = 0.012$ MPa for the seismicity between 1970 and 2003 in Japan [*Console et al.*, 2006]; and in the range of acceptable values, 0.0012–0.6 MPa, found for earthquake interactions in the San Francisco Bay Area [*Harris and Simpson*, 1998].

[26] The estimated value of the background rate r seems also to be reasonable because it lies between two independent, rough estimations based on pre-Landers earthquake activity in the region: (1) the average seismicity in the year before the M7.3 Landers main shock; and (2) the average earthquake rate, estimated from the declustered catalogue in the period 1984–1991. The declustering was performed according to *Helmstetter et al.* [2007], using the algorithm

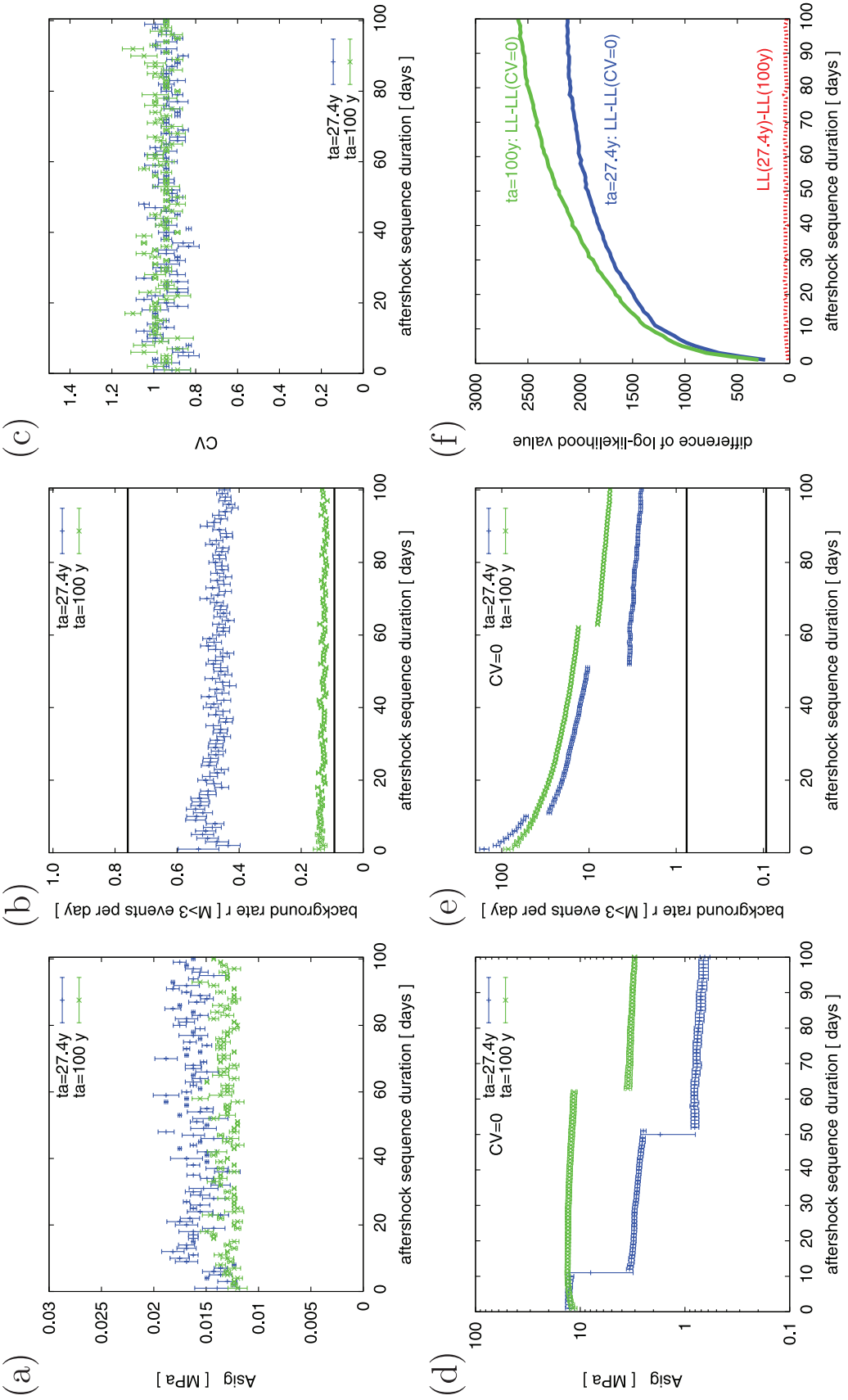

Figure 4. Variation of the model parameter estimations as a function of the time relative to the Landers main shock, for t_a = 27.4 years and t_a = 100 years. (a–c) Estimated values in the case that parameters $A\sigma_n$, r, and CV are simultaneously optimized. (d, e) Estimations in the case that only $A\sigma_n$ and r are simultaneously optimized whereas CV is set to 0. In the latter case, the parameters are plotted in a double logarithmic scale. In Figures 4b and 4e, the upper horizontal lines refer to the average rate observed in the 1 year preceding the Landers main shock, whereas the lower lines refer to the average rate of the declustered catalogue between 1984 and 1991. In Figure 4f, the differences between the log likelihood values are shown. The unstable parameter estimation and the much smaller likelihood value indicate a bad fit if stress uncertainty is ignored ($CV = 0$).

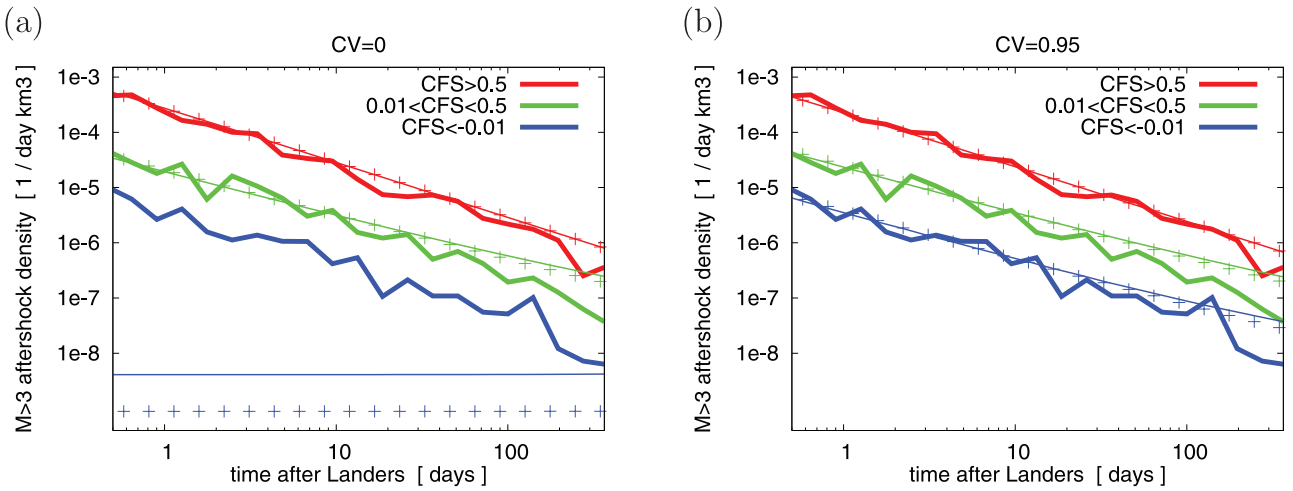

Figure 5. Comparison of the observed Landers aftershock activity (bold lines) with that of the rate-and-state model (thin lines and crosses): (a) without ($CV = 0$) and (b) with ($CV = 0.95$) consideration of stress heterogeneities. The plots show the earthquake density as a function of time in the regions of high ($\Delta CFS > 0.5$ MPa), moderate ($0.01 < \Delta CFS < 0.5$ MPa) or negative stress changes ($\Delta CFS < -0.01$ MPa), respectively. Thin lines represent the result for $t_a = 10{,}000$ days ($A\sigma_n = 0.017$ MPa, $r = 0.47$), and crosses refer to the model with $t_a = 100$ years ($A\sigma_n = 0.014$ MPa, $r = 0.13$).

by *Reasenberg* [1985]. Finally, the inverted stress heterogeneity $CV = 0.95$ is in general agreement with the results from our previous analysis in section 2.1.

3.4. Analysis of the Landers Aftershock Sequence

[27] Now we use the inverted parameters to analyze the aftershock sequence in more detail. At first we analyze the aftershock activity in different regions which experienced significant stress changes due to the Landers and Big Bear event. In particular, we consider the following three different spatial volumes in which approximately the same number of aftershocks occurred.

[28] 1. All subvolumes where the calculated stress increased by more than 0.5 MPa,

[29] 2. All subvolumes where the calculated stress increased between 0.01 and 0.5 MPa,

[30] 3. All subvolumes where the calculated stress decreased by more than 0.01 MPa.

[31] Although the total aftershock numbers were approximately the same in all of these three subvolumes, the corresponding spatial volumes are very different. The observed aftershock densities in these regions are plotted in Figure 5 (bold lines) as a function of time. As expected from theoretical point of view, the aftershock density is highest in the most stressed regions and lowest in the stress shadows. However, even in the stress shadows (i.e., in the regions where stresses are estimated to decrease due to the two major events), a clear aftershock decay according to the Omori law is observed. In agreement with previous observations by *Mallman and Zoback* [2007], this indicates that activation rather than quiescence occurred, on average, also in the apparent stress shadows.

[32] For the same volumes, we calculated the aftershock density theoretically expected from the rate-and-state model with the above inverted values: $A\sigma_n = 0.017$ MPa, $r = 0.47$, $t_a = 10000$ days without ($CV = 0$; Figure 5a) and with stress field variability ($CV = 0.95$; Figure 5b). Figure 5 clearly shows that while the aftershock decay in the regions with the highest stress increase are quite well described without accounting for stress field variability, the model completely fails for the stress shadows. On the other hand, a stress variability of $CV = 0.95$ is able to fit all regions equally well. Thus the same parameters which have been inverted for the first days of the aftershock decay by maximum likelihood method are found to reproduce the aftershock decay also on longer timescales in stress shadows as well as in regions of stress concentration. This indicates again that the model estimation is self-consistent.

[33] In Figure 5, the model results are shown for a fixed relaxation time of $t_a = 100$ years. This model predicts an even stronger stress shadow in the absence of stress heterogeneities, otherwise the fits are almost identical for the first 100 days. Slight differences between both model estimates start to emerge in the later stage as theoretically expected. Although they are fitting very well the observed aftershock data in the first approximately 20 days, both models tend to slightly overpredict the seismicity rate in the later stage.

[34] The spatial distributions of the estimated earthquake probabilities are shown in Figure 6. These maps have been calculated by integrating the forecasted earthquake rates over the first 10 days for the models with $CV = 0$ and $CV = 0.95$, respectively. The consideration of stress variability clearly leads to a broadening of the triggering zone. In the same maps, we have also plotted the epicenters of the $M > 3$ aftershocks recorded in the same time period. Visually, the predicted spatial distribution, in particular when stress heterogeneity is considered, seems to be in good agreement with the observations.

[35] Furthermore, the observed and the modeled aftershock density show also a reasonable agreement as a function of the distance d to the main shock rupture plane (Figure 7). Here the distance d is defined as the shortest distance from a location to the *Wald and Heaton* [1994] fault segments. Both, the observation and the model results based on static stress changes, are found to have a similar shape. Within the first approximately 50 km from the fault

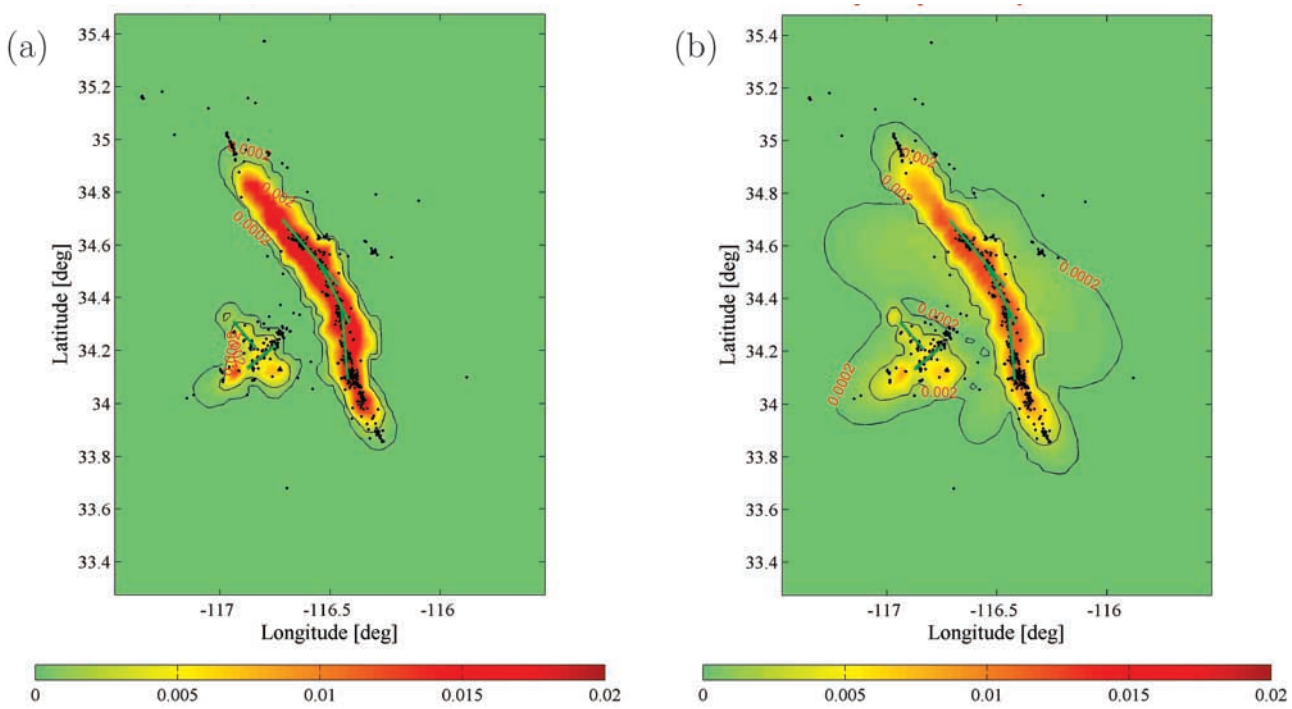

Figure 6. Spatial distribution of the aftershock probability (per 0.05 × 0.05 cell) forecasted by the model in comparison with the observed $M > 3$ aftershocks (dots) within [0.5, 10] days: (a) $CV = 0$ and (b) $CV = 0.95$. The other parameters are $t_a = 10{,}000$ days, $A\sigma_n = 0.017$ MPa, and $r = 0.47$. The Landers fault trace, indicated by bold lines, is that used by *Wald and Heaton* [1994].

plane, the decay can be approximated in both cases by $d^{-1.3}$ which is in agreement with results of *Felzer and Brodsky* [2006] for the immediate aftershocks of small main shocks. The latter analysis by Felzer and Brodsky, which is still controversially debated (K. Richards-Dinger and R. Stein, in preparation, 2009), seems to point to the triggering mechanism of dynamic stress rather than to static stress which is known to decay with d^{-3} in the far field. However, in the Landers case, we observe a bending in the far field which is in agreement with the static triggering model.

[36] In summary, the visual comparison between modeled and observed aftershocks indicates a quite good agreement. A detailed testing of the forecasting ability of the model in comparison to other Coulomb-stress based models as well as empirical models such as the ETAS [*Ogata*, 1998; *Hainzl and Ogata*, 2005; *Lombardi et al.*, 2006; *Hainzl et al.*, 2008] and STEP model [*Gerstenberger et al.*, 2005] will be performed in another paper (J. Woessner et al., A retrospective comparative test for the 1992 Landers sequence, submitted to *Journal of Geophysical Research*, 2009, hereinafter referred to as Woessner et al., submitted manuscript, 2009).

4. Discussion

[37] In this paper, we focused on the impact of the uncertainty in stress calculations, in particular, with regard to parameter estimations and forecasting of the spatiotemporal aftershock activity. Our analysis shows consistent estimations of the stress uncertainty based, firstly, on direct analysis of different published slip distributions and, secondly, on indirect results from the modeling of the recorded aftershocks. On average, the variability of stress calculations is found to be independent of the location in the order of the calculated stress value. Consequently, realistic applications of stress-based models have to take, in a probabilistic manner, the large epistemic uncertainties of

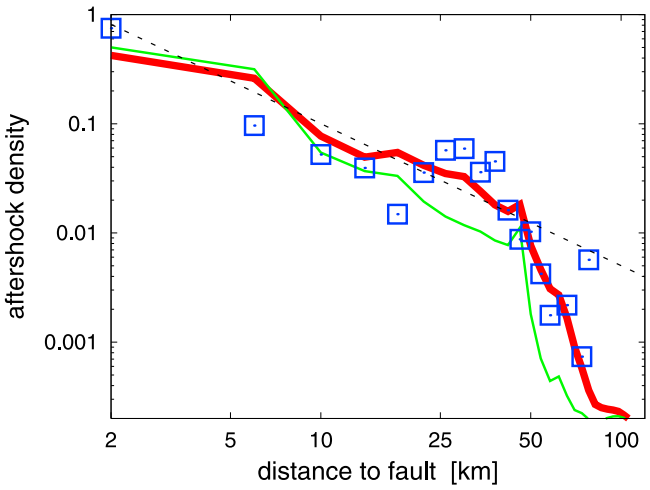

Figure 7. The spatial density of aftershocks as a function of the distance d to the fault plane of the Landers main shock: observed (squares) and predicted values with ($CV = 0.95$, bold line) and without ($CV = 0$, thin line) stress heterogeneity (the other parameters are $t_a = 10{,}000$ days, $A\sigma_n = 0.017$ MPa, and $r = 0.47$). In all cases, the values refer to the time interval [0.5, 10] days after the main shock. The dashed line refers to a decay of $d^{-1.3}$.

the slip models and the aleatoric variability due to heterogeneities into account, otherwise they will be restricted to only one of many possible stress field realizations. Our approach to introduce only one additional degree of freedom can thus be seen as the simplest attempt to take the stress field uncertainty/variability into account. The application of this basic model yielded for the Landers case (1) spatiotemporal seismicity patterns in agreement with the observations, (2) consistent maximum likelihood parameter estimations on different timescales, and (3) a consistent estimation of the stress field variability. Although this does not validate the model, it demonstrates the consistency of the model in explaining the Landers aftershock activity.

[38] While our model analysis is quite sophisticated with regard to stress heterogeneity, we made, on the other hand, a number of simplifications. Below, we mention only a few of them. A detailed discussion and comparison of the main ingredients that influence the forecasted rates is given in the paper of Cocco et al. (submitted manuscript, 2009).

[39] Firstly, the background rate cannot be expected to be constant in space as we assumed. Preexisting larger fault structures are likely to be correlated to higher background rates than regions without these features. Although this is quite obvious, we refrained in our investigations from considering such an inhomogeneity because of the practical difficulty to estimate the spatial distribution of the background activity which can introduce additional problems. To study the impact of stress uncertainties in isolation, we neglected the possible variability of the background activity in the present analysis.

[40] Another general problem of models based on stress calculations is that stress changes of secondary events are not properly considered. Aftershocks can in general influence considerably the local stress field and thus lead to a nonnegligible number of secondary aftershocks [*Ogata*, 1998; *Felzer et al.*, 2003]. Models based on Coulomb-stress can partly account for this by considering stress changes due to the largest aftershocks. In this paper, we have included the largest aftershock (M_w6.4 Big Bear earthquake) in our stress calculations.

[41] For simplification, we have also assumed that the local stress variability can be approximated by a Gaussian distribution. In section 2.2, we have shown that this is a rather good approximation for calculated stresses based on randomized slip and crustal models with Gaussian errors for slip, geometry, friction and prestress values. However, it is an open question whether this holds, if stresses would be directly calculated for a large number of different slip inversions.

[42] Finally, it is important to note that our analysis does not account for other mechanisms which might also explain the observations such as induced fluid flows and inelastic processes, i.e., afterslip. Thus we cannot prove that stress heterogeneity is the most important mechanism in this respect, however, we show that it should not be neglected in any case.

5. Summary

[43] Static Coulomb-stress changes have been mostly seen as one of the major triggering mechanisms for aftershocks. This is based on observed correlations between the spatial distributions of static stress changes and aftershock activity and the explanation of the empirically observed Omori-Utsu law by the rate- and state-dependent frictional response to static stress changes. However, static stress triggering has been recently questioned because of a number of problems: (1) the correlations between calculated stress and aftershock activity are typically not very high [e.g., *Hardebeck et al.*, 1998]; (2) aftershocks occur also in stress shadows where the model predicts a decrease in seismicity rate [e.g., *Marsan*, 2003]; and (3) the spatial decay of aftershock rates with distance to the main shock seems to indicate dynamic rather than static stress triggering [*Kilb et al.*, 2000; *Felzer and Brodsky*, 2006].

[44] Recently it has been shown from a theoretical point of view that accounting for the small-scale variability that might not be accessible neither to direct measurement nor computation, can explain the absence of regions of quiescence in the first part of the aftershock activity [*Helmstetter and Shaw*, 2006; *Marsan*, 2006] and magnitude-dependent Omori-Utsu parameters [*Hainzl and Marsan*, 2008]. This small-scale variability can result from fractal slip on the main shock rupture plane, as well as from heterogenous prestress or material conditions. However, in practice, such existing stress variability within subvolumes will be superposed by the uncertainty of our deterministic stress calculations. Coulomb-stress maps are calculated from slip models which are inverted from seismologic and geodetic measurements of the coseismic ground motion. As recently demonstrated by a blind test (see http://www.seismo.ethz.ch/staff/martin/BlindTest.html), slip inversions are often ambiguous and can significantly differ in their results even for idealized data sets [see also *Woessner et al.*, 2006]. In addition, the stress calculation itself consists of uncertain assumptions about rheological properties of the crust and the regional stress field. For the well-studied 1992 M_w7.3 Landers, California, earthquake, we have shown here by analyzing five different published slip models that this can easily lead to standard deviations which are on the order of the deterministically calculated stress value. Thus any test of the static stress triggering model must take these uncertainties into account.

[45] We explicitly considered the uncertainty in our maximum likelihood fit of the aftershock data. Our procedure is based on our finding that the stress variability is, in a first approximation, proportional to the absolute value of the stress change. Therefore we introduced only one additional parameter, namely the coefficient of variation CV which is the ratio between the standard deviation and the mean value. Using only aftershock data, we find that the parameter estimations are stable in time, which is not the case if the uncertainty is neglected. Our estimations yield reasonable values for the background rate (0.5 events with $M \geq 3$ per day in the region under consideration) as well as for the friction parameter, $A\sigma_n \approx 0.017$ MPa. Both values are in the range of independent measurements. Furthermore, the estimated stress uncertainty $CV = 0.95$ resulting from the likelihood fit is in good agreement with our independent analysis of the variability resulting from the five different slip models. These results indicate the self consistency of our estimations.

[46] The retrospective comparison of the observed spatiotemporal aftershock activity with that predicted by the

static stress triggering model, where stress heterogeneities are taken into account, indicates that none of the observations mentioned above seems to contradict the model any more. The spatiotemporal correlation is visually good, in particular, an Omori-type aftershock decay is both forecasted and observed in the regions which are in the stress shadow. Furthermore, the predicted spatial distribution is in agreement with the data. In particular, the predicted decay of the aftershock density with distance to the main shock rupture plane fits well the observed activity. These results indicate the consistency of the static stress triggering model with the observations of the Landers aftershock activity. However, as long as we have no better constraints on the stress field and the crustal properties, it might be difficult, due to the larger flexibility, to validate the model in a strict sense.

[47] In general, the consideration of uncertainties involved in the estimation of induced stress changes seems to be crucial for testing and applying models based on static stress changes. A detailed test of the forecasting ability of this model in comparison to other models, in particular, to stochastic models using only empirical laws such as the ETAS and STEP models will be presented in a follow up paper by Woessner et al. (submitted manuscript, 2009).

Appendix A

A1. Rate Evolution Due to Stress Jumps

[48] Starting from the stationary background rate r, the rate after a series of stress jumps ΔS_i at time t_i ($i = 1,\ldots, N$) can be determined by equation (3) with

$$\dot{\tau}\gamma(t) = 1 + \left(\dot{\tau}\gamma_{N-1} e^{-\frac{\Delta S_N}{A\sigma_n}} - 1\right) e^{-\frac{t-t_N}{t_a}}, \tag{A1}$$

where $\dot{\tau}\gamma_{N-1}$ is calculated iteratively by

$$\dot{\tau}\gamma_i = 1 + \left(\dot{\tau}\gamma_{i-1}\, e^{-\frac{\Delta S_i}{A\sigma_n}} - 1\right) e^{-\frac{t_{i+1}-t_i}{t_a}} \tag{A2}$$

starting from $\dot{\tau}\gamma_0 = 1$.

A2. Parameter Estimation

[49] Our applied procedure to estimate the model parameters allows to take uncertainties in the stress value as well as in the earthquake locations into account. The method is based on the maximum likelihood method where best parameters give the highest likelihood value. The likelihood function L is the joint probability function for a given model and can be constructed by multiplying the probability density function of each of the data points together. For a given time interval $[t_0, t_1]$ and spatial volume $[x_0, x_1] \times [y_0, y_1] \times [z_0, z_1]$, the log likelihood with respect to the N earthquakes occurred at times t_i and locations $\vec{x}_i$ can be determined by

$$\ln L = \sum_{i=1}^{N} \ln R(\vec{x}_i, t_i) - \int_{t_0}^{t_1}\int_{x_0}^{x_1}\int_{y_0}^{y_1}\int_{z_0}^{z_1} R(x,y,z,t)\, dx\, dy\, dz\, dt \tag{A3}$$

[*Ogata*, 1998; *Daley and Vere-Jones*, 2003].

[50] We solve the ln L function by discretization of the spatial volume. The seismogenic volume under consideration (the box region $-117.5°$W to $-115.5°$W and 33.25°N to 35.5°N and the depth interval 0.5–15.5 km) is subdivided into subvolumes of $0.05° x\ 0.05°$ horizontal extension and 1 km depth interval. There are in total $N = 27{,}000$ subvolumes. At the central point of each subvolume, the average stress change is calculated for each stress step with regard to the different slip models. For given parameters and stressing history, the rate evolution $R_n(t)$ is calculated according to equations (3) and (A1) at each grid node. To account for the location error, the value $R(\vec{x}_i, t_i)$ has to be replaced by the weighted sum $R(t_i) = \sum_{n=1}^{N} w_n R_n(t_i)$ where w_n is the probability that the ith earthquake occurred in the nth subvolume. The weights are calculated according to the Gaussian-distributed location errors given in the catalogue.

[51] To account for the uncertainty of the stress steps, we use Monte Carlo simulations. In each subvolume, we create M random series of stress jumps (in our case, we consider only the two subsequent jumps resulting from the M7.3 Landers ($k = 1$) and the M6.4 Big Bear ($k = 2$) earthquakes) by randomly selecting values ΔS_k from Gaussian distributions with mean $\langle \Delta S_k \rangle$ and standard deviation $\delta_k = CV \cdot |\langle \Delta S_k \rangle|$. Here the mean value $\langle \Delta S_k \rangle$ is the deterministically calculated stress value based on the slip models. The likelihood value L is replaced by $\bar{L} \equiv \langle L \rangle = (1/M) \sum_{i=1}^{M} L(\Delta S_k)$.

[52] For finding the parameters $A\sigma_n$ and CV which yield the maximum likelihood value, we perform a grid search in the intervals $A\sigma_n \in [0.01, 0.2]$ MPa and $CV \in [0, 5.0]$. For given parameters $A\sigma_n$ and CV, the ratio R/r can be calculated because it is independent of r. Therefore the maximization of the log likelihood function with respect to r can be solved analytically from setting $dL/dr = 0$ leading to

$$r = N \left[\int_{t_0}^{t_1}\int_{x_0}^{x_1}\int_{y_0}^{y_1}\int_{z_0}^{z_1} \frac{R(x,y,z,t)}{r}\, dx\, dy\, dz\, dt \right]^{-1} \tag{A4}$$

[53] **Acknowledgments.** We thank Shinji Toda, an anonymous referee, and the Associate Editor for helpful recommendations. We thank Martin Mai for providing us with the slip models and the SAFER-WP5 team for an effective cooperation. This work is part of the EU-project SAFER contract 036935.

References

Beeler, N. M., R. W. Simpson, S. H. Hickman, and D. A. Lockner (2000), Pore fluid pressure, apparent friction, and Coulomb failure, *J. Geophys. Res.*, *105*(B11), 25,533–25,542.

Catalli, F., M. Cocco, R. Console, and L. Chiaraluce (2008), Modeling seismicity rate changes during the 1997 Umbria-Marche sequence (central Italy) through rate- and state-dependent model, *J. Geophys. Res.*, *113*, B11301, doi:10.1029/2007JB005356.

Cocco, M., and J. R. Rice (2002), Pore pressure and poroelasticity effects in Coulomb stress analysis of earthquake interactions, *J. Geophys. Res.*, *107*(B2), 2030, doi:10.1029/2000JB000138.

Cohee, B. P., and G. C. Beroza (1994), Slip distribution of the 1992 Landers earthquake and its implications for earthquake source mechanics, *Bull. Seismol. Soc. Am.*, *84*(3), 692–712.

Console, R., M. Murru, and F. Catalli (2006), Physical and stochastic models of earthquake clustering, *Tectonophysics*, *417*, 141–153, doi:10.1016/j.tecto.2005.05.052.

Cotton, F., and M. Campillo (1995), Frequency-domain inversion of strong motions: Application to the 1992 Landers earthquake, *J. Geophys. Res.*, *100*(B3), 3961–3975.

Daley, D. J., and D. Vere-Jones (2003), *An Introduction to the Theory of Point Processes, Vol. I: Elementary Theory and Methods*, 2nd ed., Springer, New York.

Dieterich, J. H. (1994), A constitutive law for rate of earthquake production and its application to earthquake clustering, *J. Geophys. Res.*, *99*(B2), 2601–2618.

Dieterich, J. H., V. Cayol, and P. Okubo (2000), The use of earthquake rate changes as a stress meter at Kilauea volcano, *Nature*, *408*, 457–460.

Enescu, B., J. Mori, and M. Miyazawa (2007), Quantifying early aftershock activity of the 2004 mid-Niigata Prefecture earthquake (M_w6.6), *J. Geophys. Res.*, *112*, B04310, doi:10.1029/2006JB004629.

Enescu, B., J. Mori, M. Miyazawa, and Y. Kano (2009), Omori-Utsu law c-values associated with recent moderate earthquakes in Japan, *Bull. Seismol. Soc. Am.*, *99*(2A), 884–891, doi:10.1785/0120080211.

Felzer, K. R., and E. E. Brodsky (2006), Decay of aftershock density with distance indicates triggering by dynamic stress, *Nature*, *441*, 735–738.

Felzer, K. R., R. E. Abercrombie, and G. Ekstrom (2003), Secondary aftershocks and their importance for aftershock forecasting, *Bull. Seismol. Soc. Am.*, *93*(4), 1433–1448.

Gerstenberger, M. C., S. Wiemer, L. M. Jones, and P. A. Reasenberg (2005), Real-time forecasts of tomorrow's earthquakes in California, *Nature*, *435*, 328–331.

Gross, S. (2001), A model of tectonic stress state and rate using the 1994 Nothridge earthquake sequence, *Bull. Seismol. Soc. Am.*, *91*(2), 263–275.

Gross, S., and C. Kisslinger (1997), Estimating tectonic stress rate and state with Landers aftershocks, *J. Geophys. Res.*, *102*(B4), 7603–7612.

Hainzl, S., and D. Marsan (2008), Dependence of the Omori-Utsu law parameters on main shock magnitude: Observations and modeling, *J. Geophys. Res.*, *113*, B10309, doi:10.1029/2007JB005492.

Hainzl, S., and Y. Ogata (2005), Detecting fluid signals in seismicity data through statistical earthquake modeling, *J. Geophys. Res.*, *110*, B05S07, doi:10.1029/2004JB003247.

Hainzl, S., T. Kraft, J. Wassermann, H. Igel, and E. Schmedes (2006), Evidence for rainfall-triggered earthquake activity, *Geophys. Res. Lett.*, *33*, L19303, doi:10.1029/2006GL027642.

Hainzl, S., A. Christophersen, and B. Enescu (2008), Impact of earthquake rupture extensions on parameter estimations of point-process models, *Bull. Seismol. Soc. Am.*, *98*, 2066–2072.

Hardebeck, J. L., and E. Hauksson (2001), Crustal stress field in southern California and its implications for fault mechanisms, *J. Geophys. Res.*, *106*(B10), 21,859–21,882.

Hardebeck, J. L., J. J. Nazareth, and E. Hauksson (1998), The static stress change triggering model: Constraints from two southern California aftershock sequences, *J. Geophys. Res.*, *103*(B10), 24,427–24,437.

Harris, R. A. (1998), Introduction to special section: Stress triggers, stress shadows, and implications for seismic hazard, *J. Geophys. Res.*, *103*(B10), 24,347–24,358.

Harris, R. A., and R. W. Simpson (1998), Suppression of large earthquakes by stress shadows: A comparison of Coulomb and rate-and-state failure, *J. Geophys. Res.*, *103*(B10), 24,439–24,451.

Hartzell, S., L. Pengcheng, C. Mendoza, J. Chen, and K. M. Larson (2007), Stability and uncertainty of finite-fault slip inversions: Application to the 2004 Parkfield, California, earthquake, *Bull. Seismol. Soc. Am.*, *97*, 1911–1934.

Hauksson, E., W.-C. Chi, and P. Shearer (2003), Comprehensive waveform cross-correlation of southern California seismograms: Part 1. Refined hypocenters obtained using the double-difference method and tectonic implications, *Eos Trans. AGU*, Fall. Meet. Suppl., Abstract S21D-0325.

Helmstetter, A., and B. E. Shaw (2006), Relation between stress heterogeneity and aftershock rate in the rate-and-state model, *J. Geophys. Res.*, *111*, B07304, doi:10.1029/2005JB004077.

Helmstetter, A., Y. Y. Kagan, and D. D. Jackson (2005), Importance of small earthquakes for stress transfers and earthquake triggering, *J. Geophys. Res.*, *110*, B05S08, doi:10.1029/2004JB003286.

Helmstetter, A., Y. Y. Kagan, and D. D. Jackson (2007), High-resolution time-independent grid-based forecast for M $\geq$ 5 earthquakes in California, *Seismol. Res. Lett.*, *78*, 78–86.

Hernandez, B., F. Cotton, and M. Campillo (1999), Contribution of radar interferometry to a two-step inversion of the kinematic process of the 1992 Landers earthquake, *J. Geophys. Res.*, *104*(B6), 13,083–13,099.

Jones, L. E., and S. E. Hough (1995), Analysis of broadband records from the 28 June 1992 Big Bear earthquake: Evidence of a multiple-event source, *Bull. Seismol. Soc. Am.*, *85*(3), 688–704.

Kagan, Y. Y. (2004), Short-term properties of earthquake catalogs and models of earthquake source, *Bull. Seismol. Soc. Am.*, *94*(4), 1207–1228.

Kagan, Y. Y., and H. Houston (2005), Relation between mainshock rupture process and Omori's law for aftershock moment release rate, *Geophys. J. Int.*, *163*(3), 1039–1048.

Kilb, D., J. Gomberg, and P. Bodin (2000), Triggering of earthquake aftershocks by dynamic stresses, *Nature*, *408*, 570–574.

King, G. C. P., R. S. Stein, and J. Lin (1994), Static stress changes and the triggering of earthquakes, *Bull. Seismol. Soc. Am.*, *84*(1), 935–953.

Linker, J., and J. H. Dieterich (1992), Effects of variable normal stress on rock friction: Observations and constitutive equations, *J. Geophys. Res.*, *97*(B4), 4923–4940.

Lombardi, A. M., W. Marzocchi, and J. Selva (2006), Exploring the evolution of a volcanic seismic swarm: The case of the 2000 Izu Islands swarm, *Geophys. Res. Lett.*, *33*, L07310, doi:10.1029/2005GL025157.

Mallman, E. P., and M. D. Zoback (2007), Assessing elastic Coulomb stress transfer models using seismicity rates in southern California and southwestern Japan, *J. Geophys. Res.*, *112*, B03304, doi:10.1029/2005JB004076.

Marsan, D. (2003), Triggering of seismicity at short timescales following Californian earthquakes, *J. Geophys. Res.*, *108*(B5), 2266, doi:10.1029/2002JB001946.

Marsan, D. (2006), Can coseismic stress variability suppress seismicity shadows? Insights from a rate-and-state friction model, *J. Geophys. Res.*, *111*, B06305, doi:10.1029/2005JB004060.

Marsan, D., and G. Daniel (2007), Measuring the heterogeneity of the coseismic stress change following the 1999 M_w7.6 Chi-Chi earthquake, *J. Geophys. Res.*, *112*, B07305, doi:10.1029/2006JB004651.

McCloskey, J., S. S. Nalbant, S. Steacy, C. Nostro, O. Scotti, and D. Baumont (2003), Structural constraints on the spatial distribution of aftershocks, *Geophys. Res. Lett.*, *30*(12), 1610, doi:10.1029/2003GL017225.

Ogata, Y. (1998), Space-time point-process models for earthquake occurrences, *Ann. Inst. Stat. Math.*, *50*, 379–402.

Peng, Z. G., J. E. Vidale, and H. Houston (2006), Anomalous early aftershock decay rate of the 2004 Mw6.0 Parkfield, California, earthquake, *Geophys. Res. Lett.*, *33*, L17307, doi:10.1029/2006GL026744.

Peng, Z. G., J. E. Vidale, M. Ishii, and A. Helmstetter (2007), Seismicity rate immediately before and after main shock rupture from high-frequency waveforms in Japan, *J. Geophys. Res.*, *112*, B03306, doi:10.1029/2006JB004386.

Reasenberg, P. (1985), Second-order moment of central California seismicity, 1969–1982, *J. Geophys. Res.*, *90*(B7), 5479–5495.

Steacy, S., D. Marsan, S. S. Nalbant, and J. McCloskey (2004), Sensitivity of static stress calculations to the earthquake slip distribution, *J. Geophys. Res.*, *109*, B04303, doi:10.1029/2002JB002365.

Steacy, S., J. Gomberg, and M. Cocco (2005a), Introduction to special section: Stress transfer, earthquake triggering, and time-dependent seismic hazard, *J. Geophys. Res.*, *110*, B05S01, doi:10.1029/2005JB003692.

Steacy, S., S. S. Nalbant, J. McCloskey, C. Nostro, O. Scotti, and D. Baumont (2005b), Onto what planes should Coulomb stress perturbations be resolved?, *J. Geophys. Res.*, *110*, B05S15, doi:10.1029/2004JB003356.

Stein, R. S. (1999), The role of stress transfer in earthquake occurrence, *Nature*, *402*(6762), 605–609.

Toda, S., R. S. Stein, P. A. Reasenberg, J. H. Dieterich, and A. Yoshida (1998), Stress transferred by the 1995 M_w = 6.9 Kobe, Japan, shock: Effect on aftershocks and future earthquake probabilities, *J. Geophys. Res.*, *103*(B10), 24,543–24,565.

Toda, S., R. S. Stein, and T. Sagiya (2002), Evidence from the AD 2000 Izu islands earthquake swarm that stressing rate governs seismicity, *Nature*, *419*(6902), 58–61.

Toda, S., R. S. Stein, K. Richards-Dinger, and S. B. Bozkurt (2005), Forecasting the evolution of seismicity in southern California: Animations built on earthquake stress transfer, *J. Geophys. Res.*, *110*, B05S16, doi:10.1029/2004JB003415.

Utsu, T., Y. Ogata, and R. S. Matsu'ura (1995), The centenary of the Omori formula for a decay of aftershock activity, *J. Phys. Earth*, *43*, 1–33.

Wald, D. J., and T. H. Heaton (1994), Spatial and Temporal Distribution of Slip for the 1992 Landers, California, Earthquake, *Bull. Seismol. Soc. Am.*, *84*(3), 668–691.

Wang, R. J., F. Lorenzo-Martin, and F. Roth (2006), PSGRN/PSCMP—A new code for calculation co- and post-seismic deformation, geoid and gravity changes based on the viscoelastic-gravitational dislocation theory, *Comput. Geosci.*, *32*(4), 527–541.

Woessner, J., and S. Wiemer (2005), Assessing the quality of earthquake catalogues: Estimating the magnitude of completeness and its uncertainty, *Bull. Seismol. Soc. Am.*, *95*, 684–698.

Woessner, J., D. Schorlemmer, S. Wiemer, and P. M. Mai (2006), Spatial correlation of aftershock locations and on-fault main shock properties, *J. Geophys. Res.*, *111*, B08301, doi:10.1029/2005JB003961.

Zeng, Y., and J. Anderson (2000), Evaluation of numerical procedures for simulating near-fault long-period ground motions using Zeng method,

Rep. 2000/01 to the PEER Utilities Program. (Available at http://peer.berkeley.edu)

F. Catalli and M. Cocco, Sezione Sismologia e Tettonofisica Istituto Nazionale di Geofisica e Vulcanologia, Via di Vigna Murata 605, 00143 Rome, Italy. (catalli@ingv.it; cocco@ingv.it)

B. Enescu, Earthquake Research Department, National Research Institute for Earth Science and Disaster Prevention, 3-1 Tennodai, Tsukuba, Ibaraki 305-0006, Japan. (benescu@bosai.go.jp)

S. Hainzl, F. Roth, and R. Wang, Helmholtz Centre Potsdam, GFZ German Research Centre for Geosciences, Section 2.1, Telegrafenberg, D-14473 Potsdam, Germany. (hainzl@gfz-potsdam.de; roth@gfz-potsdam.de; wang@gfz-potsdam.de)

J. Woessner, Institute of Geophysics, Swiss Seismological Service, ETH Zurich, Sonneggstrasse 5, CH-8092 Zurich, Switzerland. (j.woessner@sed.ethz.ch)